

HIGH-RESOLUTION 25 μ M IMAGING OF THE DISKS AROUND HERBIG Ae/Be STARS ¹

M. HONDA², K. MAASKANT^{3,4}, Y. K. OKAMOTO⁵, H. KATAZA⁶, T. YAMASHITA⁷, T. MIYATA⁸, S. SAKO⁸, T. FUJIYOSHI⁹, I. SAKON¹⁰, H. FUJIWARA⁹, T. KAMIZUKA⁸, G. D. MULDER¹¹, E. LOPEZ-RODRIGUEZ¹², C. PACKHAM¹² AND T. ONAKA¹⁰

Draft version March 25, 2021

ABSTRACT

We imaged circumstellar disks around 22 Herbig Ae/Be stars at 25 μ m using Subaru/COMICS and Gemini/T-ReCS. Our sample consists of equal numbers of objects belonging to the two categories defined by Meeus et al. (2001); 11 group I (flaring disk) and II (flat disk) sources. We find that group I sources tend to show more extended emission than group II sources. Previous studies have shown that the continuous disk is hard to be resolved with 8 meter class telescopes in Q-band due to the strong emission from the unresolved innermost region of the disk. It indicates that the resolved Q-band sources require a hole or gap in the disk material distribution to suppress the contribution from the innermost region of the disk. As many group I sources are resolved at 25 μ m, we suggest that many, not all, group I Herbig Ae/Be disks have a hole or gap and are (pre-)transitional disks. On the other hand, the unresolved nature of many group II sources at 25 μ m supports that group II disks have continuous flat disk geometry. It has been inferred that group I disks may evolve into group II through settling of dust grains to the mid-plane of the proto-planetary disk. However, considering growing evidence for the presence of a hole or gaps in the disk of group I sources, such an evolutionary scenario is unlikely. The difference between groups I and II may reflect different evolutionary pathways of protoplanetary disks.

Subject headings: circumstellar matter — stars: pre-main sequence

1. INTRODUCTION

Recent discoveries of numerous exoplanets have been revealing the diversity of planetary systems (e.g. Marois et al. 2008). However, the origin of such variety is still uncertain. Planets should have formed in the protoplanetary disks and it is essential to understand their evolution in order to resolve why such differences exist. In studies of lower-mass young stars such as T Tauri stars, transitional disks have received attention from a view of planet formation. Transitional or pre-transitional disks are protoplanetary disks with an inner hole and/or gaps indicated by the weak near-infrared(NIR)/mid-

infrared(MIR) excess in their spectral energy distribution (SED) (Strom et al. 1989; Espaillat et al. 2007). Since a primordial protoplanetary disk must have continuous distributions of dust/gas without gaps and the disk structure will be affected by planet formation, those disks with an inner hole and/or gaps must be in a transitional phase from a primordial to an evolved planetary-system stage.

Disks around nearby Herbig Ae/Be stars have also been studied extensively in the context of the disk evolution and planet formation, but in a different classification approach. Based on an analysis of SEDs, Meeus et al. (2001) classified Herbig Ae/Be stars into two groups: group I sources, which show both a power-law and a blackbody components up to far-infrared (FIR) wavelengths in their SEDs, and group II sources, whose SEDs can be well modeled with only a single power-law from MIR to FIR wavelengths. They suggested that group I has a flaring disk, while the disk around group II is geometrically flat.

There are several scenarios proposed for an evolutionary link between groups I and II sources. Dullemond & Dominik (2004) showed that SEDs of group I sources can be interpreted as hydrostatic disks with flaring geometry, while group II sources are an evolved version of group I sources, which have undergone grain growth and grain settling to the mid-plane of the disk. Such a settled disk would become a self-shadowed disk by a puffed-up inner rim that accounts for weak FIR emission (Dullemond & Dominik 2004). Mariñas et al. (2011) performed a MIR imaging survey of Herbig Ae/Be disks at 12 and 18 μ m. They found that group I disks show more extended emission than those of group II and suggested that the trend can be naturally understood in terms of the difference in the disk geometry.

Recent high-spatial resolution observations at various

¹ Based on data collected at Subaru Telescope, via the time exchange program between Subaru and the Gemini Observatory. The Subaru Telescope is operated by the National Astronomical Observatory of Japan.

² Department of Mathematics and Physics, Kanagawa University, 2946 Tsuchiya, Hiratsuka, Kanagawa 259-1293, Japan

³ Leiden Observatory, Leiden University, PO Box 9513, 2300 RA Leiden, The Netherlands

⁴ Astronomical Institute Anton Pannekoek, University of Amsterdam, P.O. Box 94249, 1090 GE Amsterdam, The Netherlands

⁵ Institute of Astrophysics and Planetary Sciences, Faculty of Science, Ibaraki University, 2-1-1 Bunkyo, Mito, Ibaraki 310-8512, Japan

⁶ Department of Infrared Astrophysics, Institute of Space and Astronautical Science, Japan Aerospace Exploration Agency, 3-1-1 Yoshinodai, Sagami-hara, Kanagawa 229-8510, Japan

⁷ National Astronomical Observatory of Japan, 2-21-1 Osawa, Mitaka, Tokyo 181-8588, Japan

⁸ Institute of Astronomy, School of Science, University of Tokyo, 2-21-1 Osawa, Mitaka, Tokyo 181-0015, Japan

⁹ Subaru Telescope, National Astronomical Observatory of Japan, 650 North A'ohoku Place, Hilo, Hawaii 96720, U.S.A.

¹⁰ Department of Astronomy, School of Science, University of Tokyo, Bunkyo-ku, Tokyo 113-0033, Japan

¹¹ Lunar and Planetary Laboratory, The University of Arizona, Tucson, AZ 85721, USA

¹² Department of Physics & Astronomy, University of Texas at San Antonio, One UTSA Circle, San Antonio, TX 78249, USA

wavelengths have revealed a more complex structure such as a hole or gaps in disks. In particular, there is a growing evidence for the presence of a hole and/or gaps toward group I sources, such as AB Aur (Lin et al. 2006; Honda et al. 2010), HD 142527 (Fukagawa et al. 2006; Fujiwara et al. 2006; Verhoeff et al. 2011), HD 135344B (Brown et al. 2009; Grady et al. 2009), HD 36112 (Isella et al. 2010), HD 169142 (Grady et al. 2007; Honda et al. 2012), Oph IRS 48 (Geers et al. 2007), HD 100546 (Bouwman et al. 2003; Benisty et al. 2010), HD 139614 (Matter et al. 2014), and HD 97048 (Maaskant et al. 2013). Recently, Honda et al. (2012) and Maaskant et al. (2013) proposed that group I sources possess a disk with a strongly depleted inner region (i.e. a transitional disk). Such a discontinuous structure is different from the one originally proposed for group I disks. As little/no evidence for a hole and/or gaps is reported toward group II disks and they seem to have a radially continuous structure, previous interpretation on an evolutionary path from group I to group II needs to be reconsidered.

In this paper, we present results of an imaging survey of nearby (roughly within 200 pc) Herbig Ae/Be stars at $24.5\ \mu\text{m}$ using the 8.2-m Subaru Telescope and 8.1-m Gemini Telescope. At $24.5\ \mu\text{m}$, the point spread function (PSF) is relatively stable compared to those at shorter wavelengths because of a larger Fried length, which enables us to discuss small extended structures with high reliability. In addition, it allows us to investigate the cooler outer part of the disk at a dust temperature ~ 100 K. Early examples of our imaging survey have been published (Fujiwara et al. 2006; Honda et al. 2010, 2012; Maaskant et al. 2013). This paper gives a summary of the survey.

2. OBSERVATIONS AND DATA REDUCTION

2.1. Subaru/COMICS data

We made imaging observations of Herbig Ae/Be stars using COMICS (Cooled Mid-Infrared Camera and Spectrometer; Kataza et al. 2000; Okamoto et al. 2003; Sako et al. 2003) on the 8.2-m Subaru Telescope with the Q24.5 filter ($\lambda_c=24.5\ \mu\text{m}$, $\Delta\lambda=0.8\ \mu\text{m}$). We also observed part of the targets with the Q18.8 filter ($\lambda_c=18.8\ \mu\text{m}$, $\Delta\lambda=0.8\ \mu\text{m}$). The chopping throw was $10''$ and the chopping frequency was 0.45 Hz. The pixel scale is $0.130''/\text{pix}$. Immediately before and/or after the observations of the target, we made observations of PSF reference stars. A summary of the observations is given in Table 1.

For the data reduction, we employed a shift-and-add method to rectify the blurring caused by tracking and/or registration errors. The imaging data consist of 0.983 sec on-source integration frames of coadded-exposures at each beam position. First, the fluctuation of the thermal background and the dark current signals were removed by the differentiation of the chopped pair frames. The object is bright enough to be recognized even in 0.983 sec integration chop-subtracted frames. We estimated the peak position of the source by a Gaussian fitting without difficulty. Then we shifted the frames so as to align the peak position and summed up the frames. We excluded the frames whose Gaussian full-widths at half-maximum (FWHMs) deviate more than $1\ \sigma$ from the mean value.

2.2. Gemini/T-ReCS data

Observations were performed using T-ReCS (Telesco et al. 1998) on the 8.1-m Gemini South telescope. T-ReCS uses a Raytheon 320×240 pixel Si:As IBC array, with a pixel scale of $0.08633 \pm 0.00013''$ pixel^{-1} , providing a field of view (FOV) of $27.6'' \times 20.7''$. The Q_b ($\lambda_c = 24.56\ \mu\text{m}$, $\Delta\lambda = 0.94\ \mu\text{m}$, 50% cut-on/off) filter was used in the present observations. A summary of the observations is shown also in Table 1. Observations were made using a standard chop-nod technique to remove time-variable sky background and telescope thermal emission, and to reduce the effect of $1/f$ noise from the array-electronics. In all observations the chop-throw was $15''$, the chop-angle 45° E of N, and the telescope was nodded approximately every 40 s. Standard stars were observed immediately before and/or after each object observation using the same instrumental configuration.

The data were reduced using the Gemini IRAF package. The difference for each chopped pair was calculated and a pair of the nod sets were then differentiated and combined to create a single image. All the nodding data were examined if they had high background due either to the presence of terrestrial clouds or temporarily high water vapor precipitation. No data were found to be severely affected by these problems.

Although there is a slight difference in the characteristics of the filters used by COMICS and T-ReCS, we will refer to Q24.5 and Q_b as $25\ \mu\text{m}$ throughout this paper.

3. RESULTS

Since the observed images show circularly-symmetric shape and the azimuthal variation is not significant, we focus on the radial profile of the targets and do not discuss azimuthal structures in this study. We first made azimuthally-averaged radial profiles of the targets and relevant PSF stars at $25\ \mu\text{m}$ as shown in Figure 1. We then measured their FWHMs from the profiles directly; we call these ‘direct FWHMs’ ($\Phi_{d,target}$ and $\Phi_{d,PSF}$ for the targets and PSFs, respectively). These FWHMs are the real extension of the sources convolved with the instrumental FWHM. These measurements are summarized in Table 2 accompanied with those of the corresponding PSF stars.

The radial brightness profiles of most targets are comparable to or slightly wider compared to that of the PSF stars. As a quantitative measure of the intrinsic size of the MIR emission from the disk, we employ a quadrature-subtraction of the FWHM of the PSF star from that of the target following Mariñas et al. (2011). We call this ‘intrinsic FWHM’ (Φ_i), which is derived from

$$\Phi_i = \sqrt{\Phi_{d,target}^2 - \Phi_{d,PSF}^2}.$$

Although this method provides a correct size only when the intrinsic radial profiles of both target and the PSF star are given by a Gaussian, we adopt this method to semi-quantitatively discuss the extension of the sources with the same measure for the sake of simplicity. Eight sources are observed by both COMICS and T-ReCS, and the results were consistent with each other within the measurement errors. To be conservative, we adopt the smaller and more stringent value of the intrinsic FWHM

on these cases. The derived values are summarized in Table 3.

4. DISCUSSION

4.1. Trends on the extended emission

To investigate possible trends of the 25 μm extension of the Herbig Ae/Be stars with other parameters, we collected the distance, stellar luminosity, classification of the group proposed by Meeus et al. (2001), and the MIR spectral index given by the flux density ratio at 13.5 and 30 μm (Acke et al. 2004; Acke & van den Ancker 2006; Acke et al. 2010; Meeus et al. 2012). The flux densities at 13.5 and 30 μm reflect the underlying continuum shape and are chosen to avoid MIR dust features such as silicates and polycyclic aromatic hydrocarbons (PAHs). For the objects whose spectral index is not available, we calculated it ourselves using the *ISO* or *Spitzer* archive spectra. We also converted the diameter in arcseconds to AU using the distance to the objects given in Table 3. We added AB Aur, which was part of our survey but its results were published earlier in Honda et al. (2010), to Table 3.

We notice that group I sources tend to show more extended MIR emission than group II sources. Nine out of 11 group I sources are resolved (i.e., 82%) with a signal-to-noise ratio (S/N) larger than three, and so are 4 out of 11 group II sources, which, however, is only 36%. This trend is similar to the results of the study by Mariñas et al. (2011) at 12 and 18 μm . The present results confirm the trend also at 25 μm .

In Figure 2, we plot the intrinsic FWHM (Φ_i) against the stellar luminosity (L_*). One may expect that luminous sources show more extended emission, however, we could not find clear trend in the plot. Some sources in our sample are not resolved even though they are luminous ($L_* > 40L_\odot$).

On the other hand, when we plot the intrinsic FWHM against the MIR spectral index (Figure 3), we find that significantly extended (FWHM > 40 AU) sources all belong to ‘red’ group I. Such objects exhibit the MIR spectral indices [30/13.5] larger than 4.2, while moderately extended or unresolved sources all show below that value, even amongst group I. It is also interesting to note that the MIR spectral indices of well-resolved MIR disk sources such as HD142527 (Fujiwara et al. 2006), Oph IRS48 (Geers et al. 2007), and HD141569 (Fisher et al. 2000; Marsh et al. 2002) are 5, 10.4, and 6.8, respectively, in accordance with the present finding. We therefore suggest that the redder Herbig Ae/Be stars with the MIR spectral index larger than 4.2 exhibit more extended MIR emission. In general, group I sources tend to show MIR continuum emission redder than those in group II. Thus the present finding is consistent with the trend that group I sources are likely to exhibit more extended emission than group II sources.

4.2. Origin of extended emission of MIR red source

The origin of Q -band (16–25 μm) extended emission of the group I Herbig Ae/Be stars or red MIR sources have so far been discussed by several groups. Honda et al. (2010, 2012) and Maaskant et al. (2013) demonstrate the difficulty in explaining the extended Q -band emission of group I sources with a continuous disk. The Q -band

emission from a continuous disk is mostly originated from dust grains located in the inner ≤ 10 AU, which corresponds to $\sim 0.07''$, if located at a typical distance of ~ 150 pc to our targets. Considering the PSF size ($\sim 0.7''$) at 25 μm , this is too small to be resolved with 8 meter class telescopes. This situation may apply to most unresolved targets in our sample. In contrast, we have definitely resolved many group I sources, indicating that the continuous disk interpretation is not valid for these objects.

The shape of SEDs for group I sources can be interpreted as having a MIR dip because of the rising FIR emission. The dip indicates that hot/warm dust grains responsible for the MIR radiation are depleted in the inner region of the protoplanetary disk. An inner hole and/or gaps in the disk can naturally explain both the MIR dip in the SED and the extended emission in the Q -band. The presence of an inner hole, for example, causes the inner edge of the disk to be directly illuminated by the central star. This edge, being relatively further away because of the inner hole, produces the red MIR index (i.e., a large [30/13.5] ratio) and the strong FIR radiation as reflected in the SED, as well as the extended Q -band emission. In fact, significantly extended sources (intrinsic FWHM > 40AU) in our sample exhibit MIR spectral indices [30/13.5] larger than 4.2, indicating that the dust temperature of the inner edge of the outer disk to be ~ 155 K assuming a blackbody. Were the luminosity of the central star 30 L_\odot (a typical value for well extended group I sources), the distance to the 155-K blackbody would be at about 18 AU, indicating an inner hole diameter of 36 AU, which corresponds to approximately 0.24'' if located at a typical distance of 150 pc. An emission region of this size, when convolved with the PSF of the telescope, can be (marginally) resolved with 8-meter class telescopes in the Q -band. We suggest that this applies to our resolved sample.

This interpretation is supported by an increasing number of detections of inner holes and gaps in group I protoplanetary disks by high-spatial resolution observations in the NIR and at radio wavelengths as described in section 1. On the other hand, little evidence has been reported for inner holes and/or gaps towards group II sources, which is also consistent with the present results of unresolved or limited extended emission. Continuous disks seem to be rather difficult to resolve in the Q -band with 8-m class telescopes.

In general, group I sources tend to show redder MIR continuum emission than group II sources. In our sample, most group I sources show the MIR spectral index higher than 2, while that of most group II objects is below 2. This is consistent with a recent classification criterion put forward by Khalefnejad et al. (2014) that the MIR index [30/13.5] of group I sources is greater than 2.1. A blackbody at $T \sim 195$ K would yield a MIR index of 2. Thus the dust temperature of the inner edge of the outer disk around group I objects must be below 195 K, which puts the inner edge at some distance from the central star, producing an extended Q -band emission. Both the high MIR index and the extended Q -band emission can naturally be accounted for by the presence of the inner edge of the outer disk located at some distance. As mentioned earlier, there is now growing evidence that an inner hole and/or gaps exist in the protoplanetary disk of group I sources. Our finding above (the general trend be-

tween the extended Q-band emission and the MIR color for group I objects) also appears to reconfirm this view.

4.3. Comparison with models

To show the effect of a gap in the disk on the Q-band image size, we constructed disk models and derived FWHM of the disk image at $25\ \mu\text{m}$ for comparison with the observations. We follow the model used in Maaskant et al. (2013) who employed the radiative transfer tool MCMAX (Min et al. 2009). Parameters used in this model are summarized in Table 4. We focus on the model with these typical Herbig Ae parameters as an example only, and we are not going to construct models that best predict individual imaging results.

First, we constructed a continuous disk model (no gap) whose SED has a rising FIR flux density similar to the group I objects. The model image at $25\ \mu\text{m}$ is displayed in the top panel of Fig.4, and the SED in Fig.5. Then we introduced a radial gap in this model. The gap inner radius is fixed at 1 AU, and the gap outer radius was increased from 10 to 50 AU in a 10-AU interval. Images and SEDs for these models are shown in Fig.4 and Fig.5, respectively. The morphology of the gapped disk images is dominated by a ring-like emission arising from the inner edge of the outer disk (see top panels of Fig.4). As the size of the gap is increased, more thermal radiation from the increasingly larger gapped area is removed from the SED, resulting in a weakened MIR emission and an enhanced FIR flux (see Fig.5). This in turn was reflected in a growingly redder $[30/13.5]$ colour as the gap size widened. The disk images were subsequently convolved with an Airy pattern with a $\text{FWHM} = 0.65''$ (assumed to represent the telescope beam; see bottom panels of Fig.4). We measured Φ_d and derived Φ_i from these final images in the same manner as described in Section 3 (see Fig.6). As can be seen, the models with outer gap radii smaller than 20 AU are comparable with the ‘no-gap’ model (equivalent within uncertainties), implying that they would either be unresolved or only marginally resolved at best. On the other hand, when the outer gap radius $\gtrsim 30$ AU, they would easily be resolved at $25\ \mu\text{m}$. Thus our $25\ \mu\text{m}$ imaging survey is sensitive to the presence of a large ($\gtrsim 30$ AU) gap. Fig.7 is the same as Fig.3, except we added the models points. In our sample models, disks with $[30/13.5] \gtrsim 4.2$ can be achieved when the gap outer radius becomes $\gtrsim 25$ AU and such disk can be well-resolved in our observations. This trend is almost consistent with our observational findings that the well-extended Herbig Ae/Be sources show MIR index larger than 4.2. Again, it demonstrates that our $25\ \mu\text{m}$ imaging survey is sensitive to disks with large gaps.

4.4. Group I sources as (pre-)transitional disks

Since the presence of an inner hole and/or gaps has been shown to be a common characteristic for group I Herbig Ae/Be stars (e.g. Lin et al. 2006; Fukagawa et al. 2006; Fujiwara et al. 2006; Verhoeff et al. 2011; Brown et al. 2009; Grady et al. 2007, 2009; Isella et al. 2010; Honda et al. 2010, 2012; Geers et al. 2007; Bouwman et al. 2003; Benisty et al. 2010; Matter et al. 2014; Maaskant et al. 2013), Honda et al. (2012) and Maaskant et al. (2013) suggest that most group I sources can be classified as (pre-)transitional disks. Transitional or pre-transitional disks, which are originally suggested for low-mass young stars such as T-Tauri stars, are protoplanetary disks with an inner hole and/or gaps indicated by the weak NIR excess in the SED (Strom et al. 1989; Espaillat et al. 2007). Because the primordial disk is thought to have a continuous distribution of dust without gaps and because planet formation could produce a hole and/or gaps in the disk, those disks with (large) inner hole and/or gaps must be in a transitional phase from a primordial to an evolved stage.

On the other hand, an evolutionary scenario for Herbig Ae/Be stars is still a matter of debate. Meeus et al. (2001) proposed that group I disk is flared while that of group II is flat, based on the analysis of the SED. A possible evolutionary scenario was suggested in which group I flaring disk evolves into group II flat disk by grain growth and sedimentation/settling of grains to the disk mid-plane. However, the present study indicates that the group I disk is a (pre-)transitional disk with an inner cleared region and/or gaps, while the group II disk is a continuous disk. These observational pieces of information imply that evolution from group I into group II is unlikely. As Meeus et al. (2001) pointed out that there is no significant difference of the age between groups I and II, it is more likely that both sources may have evolved differently from a primordial continuous flaring disk, a common ancestor as discussed in Maaskant et al. (2013). This scenario is quite similar to the T Tauri disk evolutionary scenario proposed by Currie (2010). He presented two main pathways for the evolution of T Tauri disks: those that form an inner hole/gap and others that deplete more homogeneously. The present study suggests a similarity between the evolutionary scenarios of T Tauri and Herbig Ae/Be disks.

We are grateful to all of the staff members of the Subaru Telescope. We also thank Dr. Hitomi Kobayashi and Dr. Yuji Ikeda at Kyoto-Nijikoubou Co., Ltd.. This research was partially supported by KAKENHI (Grant-in-Aid for Young Scientists B: 21740141) by the Ministry of Education, Culture, Sports, Science and Technology (MEXT) of Japan.

REFERENCES

- Acke, B., van den Ancker, M. E., Dullemond, C. P., van Boekel, R., & Waters, L. B. F. M. 2004, *A&A*, 422, 621
 Acke, B., & van den Ancker, M. E. 2006, *A&A*, 457, 171
 Acke, B., Bouwman, J., Juhász, A., et al. 2010, *ApJ*, 718, 558
 Benisty, M., Tatulli, E., Ménard, F., & Swain, M. R. 2010, *A&A*, 511, A75
 Bouwman, J., de Koter, A., Dominik, C., & Waters, L. B. F. M. 2003, *A&A*, 401, 577
 Brown, J. M., Blake, G. A., Qi, C., et al. 2009, *ApJ*, 704, 496
 Currie, T. 2010, arXiv:1002.1715
 Cohen, M., Walker, R. G., Carter, B., Hammersley, P., Kidger, M., Noguchi, K. 1999, *AJ*, 117, 1864
 Dullemond, C. P., & Dominik, C. 2004, *A&A*, 417, 159
 Dullemond, C. P., & Dominik, C. 2004, *A&A*, 421, 1075
 Espaillat, C., Calvet, N., D’Alessio, P., et al. 2007, *ApJ*, 670, L135
 Fisher, R. S., Telesco, C. M., Piña, R. K., Knacke, R. F., & Wyatt, M. C. 2000, *ApJ*, 532, L141
 Fujiwara, H., et al. 2006, *ApJ*, 644, L133

TABLE 1
SUMMARY OF SUBARU/COMICS AND GEMINI/T-RECS OBSERVATIONS

Object	Subaru/COMICS Q24.5 imaging			Subaru/COMICS Q18.8 imaging			Gemini/T-ReCS Qb imaging		
	Date	t ^a	PSF	Date	t ^a	PSF	Date	t ^a	PSF
Elias3-1	Jul 11, 2004, Jul 12, 2004	399	β And
HD100546	Jun 27, 2011	638	γ Cru
HD135344B	Jun 14, 2011	1361	α Cen A
HD139614	Jul 11, 2004	101	δ Oph	Jul 23, 2011	638	α Tra
HD169142	Jul 22, 2011	638	η Sgr
HD179218	Jul 11, 2004	99	α Her
HD36112	Dec 14, 2005, Jan 26, 2011	3297	α Tau	Jan 26, 2011	438	α Tau
HD97048	Jun 28, 2011	638	γ Cru
RCrA	Jul 11, 2004	100	δ Oph	Jul 12, 2004	40	α Her	Jun 28, 2011	203	η Sgr
TCrA	Jul 11, 2004	312	α Her	Jul 12, 2004	175	α Her	Jul 21, 2011	638	η Sgr
51 Oph	Jul 11, 2004	237	δ Oph	Jul 21, 2011	638	η Sgr
AK Sco	Jul 22, 2011	638	η Sgr
CQTau	Dec 15, 2005	553	α Tau	Dec 15, 2005	541	α Tau
HD142666	Jul 11, 2004	148	δ Oph	Jul 21, 2011	638	η Sgr
HD144432	Jul 11, 2004	193	δ Oph	Jul 24, 2011	638	δ Oph
HD150193	Jul 12, 2004	168	α Her	Jul 27, 2011	638	η Sgr
HD163296	Jul 11, 2004, Jul 12, 2004	557	δ Oph	Jun 28, 2011	638	η Sgr
HD31648	Dec 14, 2005	1510	α Tau	Dec 15, 2005	578	α Tau
HD35187	Dec 14, 2005, Dec 16, 2005	1580	α Tau
HR5999	Jul 24, 2011	638	α Tra
KK Oph	Jul 21, 2011	638	η Sgr

^a Total integration time in seconds used in this study

- Fukagawa, M., Tamura, M., Itoh, Y., Kudo, T., Imaeda, Y., Oasa, Y., Hayashi, S. S., & Hayashi, M. 2006, ApJ, 636, L153
- Geers, V. C., Pontoppidan, K. M., van Dishoeck, E. F., et al. 2007, A&A, 469, L35
- Grady, C. A., Schneider, G., Hamaguchi, K., et al. 2007, ApJ, 665, 1391
- Grady, C. A., et al. 2009, ApJ, 699, 1822
- Honda, M., Inoue, A. K., Okamoto, Y. K., et al. 2010, ApJ, 718, L199
- Honda, M., Maaskant, K., Okamoto, Y. K., et al. 2012, ApJ, 752, 143
- Isella, A., Natta, A., Wilner, D., Carpenter, J. M., & Testi, L. 2010, ApJ, 725, 1735
- Kataza, H., Okamoto, Y., Takubo, S., Onaka, T., Sako, S., Nakamura, K., Miyata, T., & Yamashita, T. 2000, Proc. SPIE, 4008, 1144
- Khalefnejad, et al. in preparation
- Lin, S.-Y., Ohashi, N., Lim, J., Ho, P. T. P., Fukagawa, M., & Tamura, M. 2006, ApJ, 645, 1297
- Mariñas, N., Telesco, C. M., Fisher, R. S., Packham, C. 2011, ApJ, 737, 57
- Marois, C., Macintosh, B., Barman, T., et al. 2008, Science, 322, 1348
- Marsh, K. A., Silverstone, M. D., Becklin, E. E., et al. 2002, ApJ, 573, 425
- Maaskant, K. M., Honda, M., Waters, L. B. F. M., et al. 2013, A&A, 555, A64
- Matter, A., Labadie, L., Kreplin, A., et al. 2014, A&A, 561, A26
- Meeus, G., Waters, L. B. F. M., Bouwman, J., van den Ancker, M. E., Waelkens, C., & Malfait, K. 2001, A&A, 365, 476
- Meeus, G., Montesinos, B., Mendigutía, I., et al. 2012, A&A, 544, A78
- Min, M., Dullemond, C. P., Dominik, C., de Koter, A., & Hovenier, J. W. 2009, A&A, 497, 155
- Okamoto, Y. K., Kataza, H., Yamashita, T., Miyata, T., Sako, S., Takubo, S., Honda, M., & Onaka, T. 2003, Proc. SPIE, 4841, 169
- Sako, S., et al. 2003, PASP, 115, 1407
- Strom, K. M., Strom, S. E., Edwards, S., Cabrit, S., & Skrutskie, M. F. 1989, AJ, 97, 1451
- Telesco, C. M., Pina, R. K., Hanna, K. T., Julian, J. A., Hon, D. B., Kisko, T. M. 1998, Proc. SPIE, 3354, 534
- Verhoeff, A. P., Min, M., Pantin, E., et al. 2011, A&A, 528, A91

TABLE 2
FWHM MEASUREMENTS OF COMICS AND T-RECS OBSERVATIONS

object	Subaru/COMICS Q24.5 imaging			Subaru/COMICS Q18.8 imaging			Gemini/T-ReCS Qb imaging		
	$\Phi_{d,target}(\prime\prime)$	$\Phi_{d,PSF}(\prime\prime)$? ^a	$\Phi_{d,target}(\prime\prime)$	$\Phi_{d,PSF}(\prime\prime)$? ^a	$\Phi_{d,target}(\prime\prime)$	$\Phi_{d,PSF}(\prime\prime)$? ^a
Elias3-1	0.672±0.012	0.634±0.003	Y
HD100546	0.788±0.006	0.716±0.008	Y
HD135344B	0.804±0.008	0.721±0.004	Y
HD139614	0.643±0.031	0.633±0.011	N	0.711±0.005	0.710±0.007	N
HD169142	0.759±0.014	0.692±0.007	Y
HD179218	0.637±0.009	0.645±0.004	N
HD36112	0.751±0.009	0.649±0.003	Y	0.559±0.017	0.526±0.027	N
HD97048	0.788±0.014	0.714±0.005	Y
RCrA	0.687±0.016	0.629±0.020	Y	0.547±0.011	0.489±0.008	Y	0.771±0.028	0.704±0.011	Y
TCrA	0.748±0.013	0.634±0.002	Y	0.586±0.026	0.489±0.004	Y	0.806±0.023	0.732±0.003	Y
51 Oph	0.663±0.037	0.626±0.006	N	0.730±0.012	0.721±0.007	N
AK Sco	0.695±0.024	0.692±0.005	N
CQTau	0.687±0.023	0.627±0.004	Y	0.519±0.005	0.501±0.011	Y?
HD142666	0.710±0.063	0.637±0.008	N	0.741±0.008	0.714±0.005	Y
HD144432	0.652±0.031	0.639±0.006	N	0.691±0.014	0.690±0.005	N
HD150193	0.728±0.081	0.641±0.002	N	0.696±0.008	0.700±0.007	N
HD163296	0.649±0.011	0.632±0.003	Y?	0.705±0.008	0.711±0.006	N
HD31648	0.677±0.013	0.646±0.006	Y	0.503±0.007	0.493±0.007	N
HD35187	0.689±0.010	0.649±0.002	Y
HR5999	0.709±0.009	0.728±0.012	N
KK Oph	0.721±0.012	0.722±0.007	N

^a Resolved(Y) or not(N)

TABLE 3
SUMMARY OF PARAMETERS OF THE SAMPLES.

Object	Distance(pc)	$L_*(L_\odot)$	Ref.	$\Phi_i(\prime\prime)$	$\Phi_i(AU)$	Group	Ref.	[30/13.5]	Ref.
AB Aur	139.3	33.0	b	0.50±0.05	70.2±6.91	I	a	4.5	a
Elias3-1	160	0.7	d	0.22±0.04	35.5±6.1	I	c	2.3	e
HD100546	96.9	22.7	b	0.33±0.02	31.7±2.3	I	a	3.5	a
HD135344B	142	8.1	b	0.36±0.02	50.6±2.7	I	a	10.9	a
HD139614	140	7.6	b	0.04±0.17	5.3±24.0	I	a	4.2	a
HD169142	145	9.4	b	0.31±0.04	45.1±5.4	I	a	7.8	a
HD179218	240	100.0	d	<0.12	<28.81	I	a	2.4	a
HD36112	279.3	33.7	b	0.38±0.02	105.6±5.5	I	a	4.1	a
HD97048	158.5	30.7	b	0.33±0.03	52.8±5.5	I	a	5.9	a
R CrA	130	0.6	d	0.31±0.07	40.9±9.5	I	c	2.1	e
T CrA	130	0.7	d	0.34±0.06	43.8±7.2	I	a	5	a
51 Oph	124.4	285.0	b	0.11±0.09	13.7±11.4	II	a	0.59	a
AK Sco	150	8.9	d	0.06±0.27	9.6±40.1	II	a	3.3	a
CQTau	113	3.4	b	0.28±0.06	31.5±6.4	II	b	4.1	e
HD142666	145	13.5	b	0.20±0.04	28.7±5.3	II	a	1.53	a
HD144432	145	10.2	d	0.05±0.23	6.6±33.5	II	a	1.82	a
HD150193	216.5	48.7	b	<0.17	<37.3	II	a	1.42	a
HD163296	118.6	33.1	b	<0.16	<19.2	II	a	2	a
HD31648	137	13.7	b	0.20±0.05	27.3±6.3	II	a	1.19	a
HD35187	114.2	17.4	b	0.23±0.03	26.5±3.4	II	a	2.1	a
HR5999	210	87.1	d	<0.11	<23.6	II	a	0.96	a
KK Oph	260	13.7	b	<0.23	<58.9	II	a	1.04	a

REFERENCES. — (a) Acke et al. 2010 (b) Meeus et al. 2012 (c) Acke & van den Ancker 2006 (d) Acke et al. 2004 (e) derived from the archival spectra

TABLE 4
PARAMETERS USED IN THE MODEL

parameter	values
stellar paramters :	
stellar effective temperature T_*	9280 K
stellar mass M_*	$2.4 M_\odot$
stellar luminosity L_*	$40. L_\odot$
distance d	144. pc
disk component :	
dust composition	80% silicates + 20% carbon
dust minimum size a_{min}	$0.1 \mu\text{m}$
dust minimum size a_{max}	1. mm
index of dust size power law	3.75
dust mass	$5 \times 10^{-5} M_\odot$
disk inner radius r_{in}	0.3 AU
disk outer radius r_{out}	400. AU
disk inclination	35°
halo component :	
dust composition	100% carbon
dust minimum size a_{min}	$0.1 \mu\text{m}$
dust minimum size a_{max}	$1. \mu\text{m}$
index of dust size power law	3.5
dust mass	$1.0 \times 10^{-12} M_\odot$
halo inner radius r_{in}	0.25 AU
halo outer radius r_{out}	0.35 AU

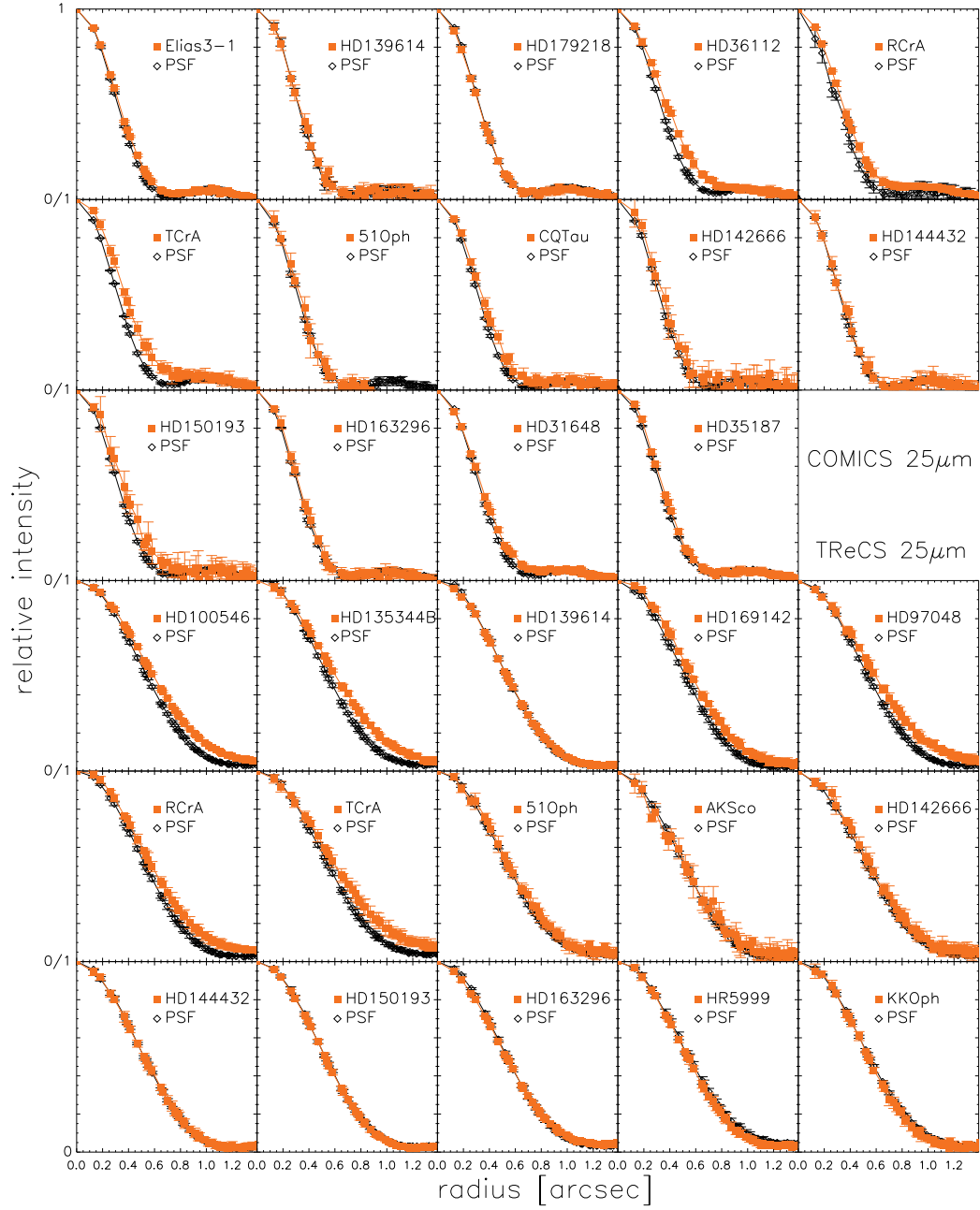


FIG. 1.— Peak-normalized azimuthally averaged radial profile plot of the targets and PSF stars at $25\mu\text{m}$. The panels of upper 3 rows are from COMICS observations, while those of lower 3 rows are from T-ReCS observations.

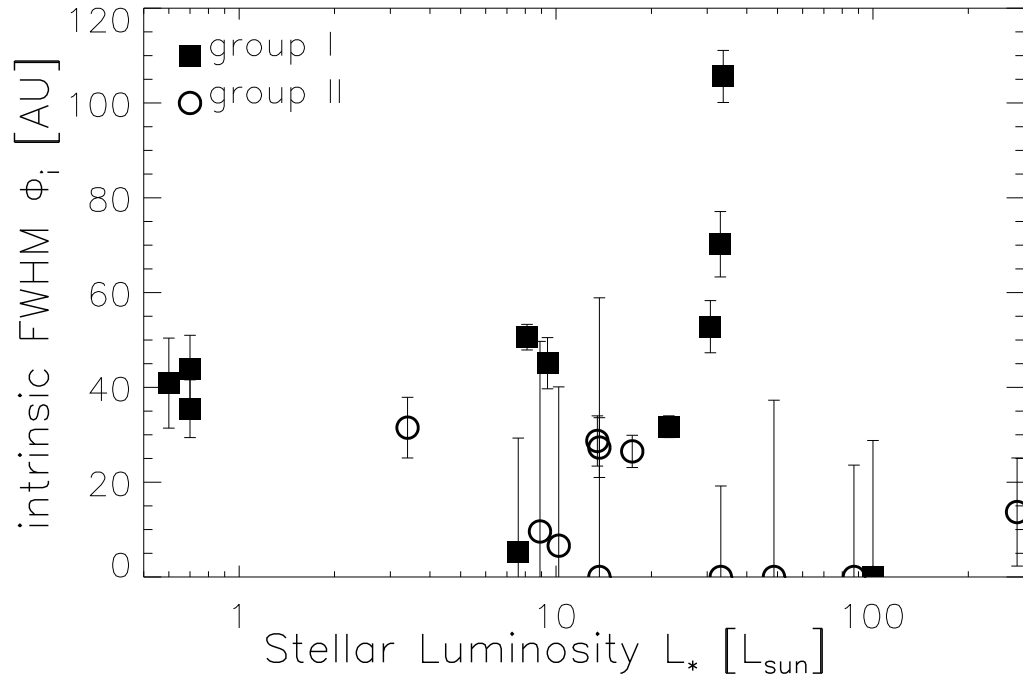


FIG. 2.— Intrinsic FWHM of extended emission at 25 μm against the stellar luminosity. The squares indicate group I sources, while the circles show group II sources. The points plotted at FWHM value of zero are those of unresolved sources with 3-sigma upper limits.

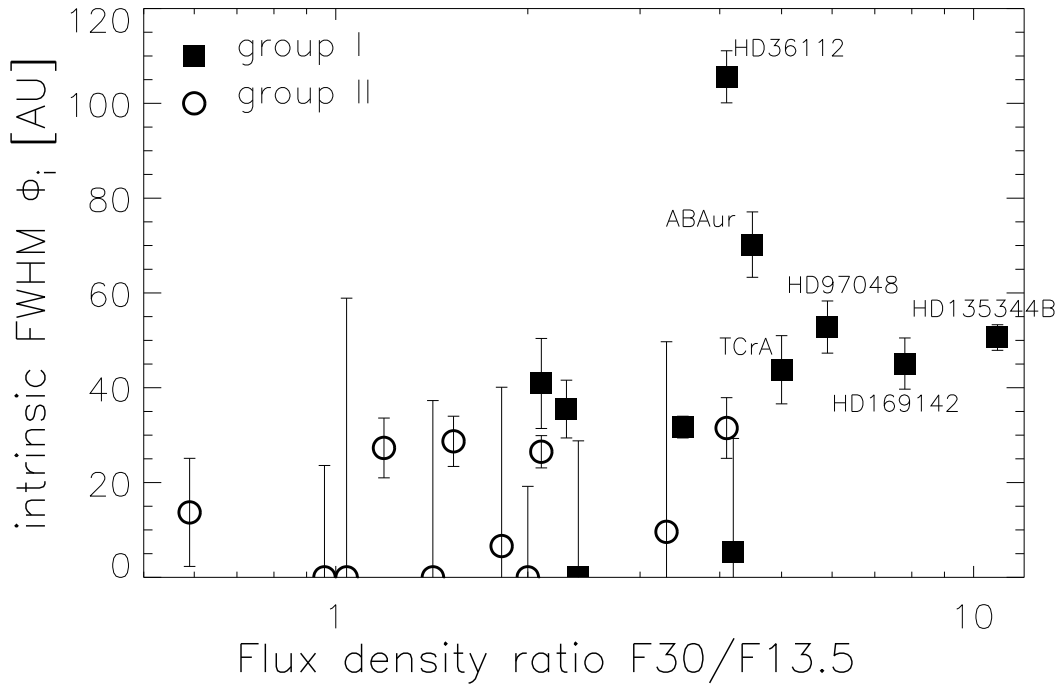


FIG. 3.— Intrinsic FWHM of extended emission at 25 μm against the MIR continuum flux ratio $F_{30}/F_{13.5}$. The symbols are the same as in Figure 2. Redder sources tend to show larger FWHM value.

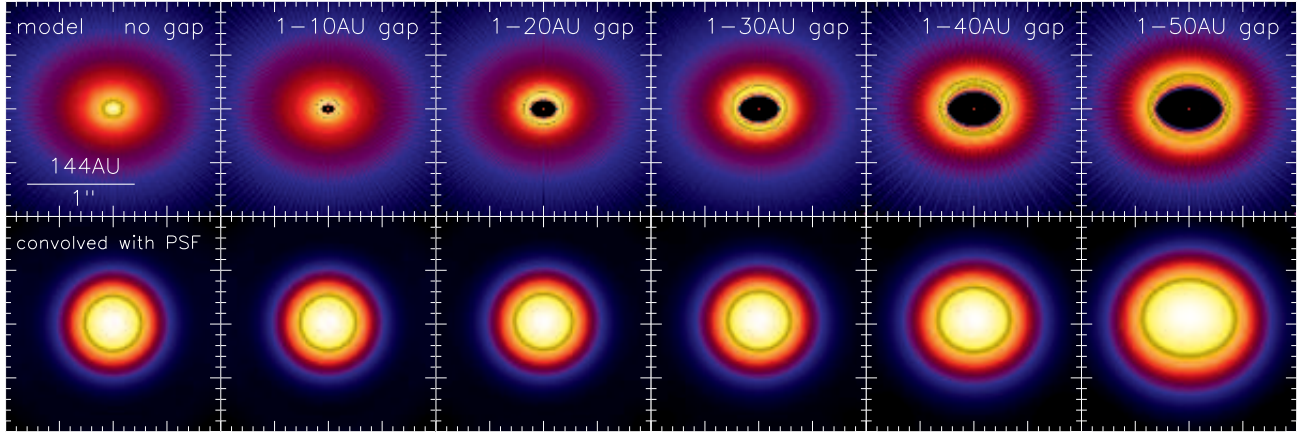


FIG. 4.— (Top) Model images of a Herbig Ae disk with typical parameters by changing gap outer radius at $25\mu\text{m}$. Images are shown in logarithmic scale to show faint outer disk emission. (Bottom) Model images convolved with the PSF, assumed to be a Airy function, with a FWHM of $0.65''$. Images are shown in linear scale.

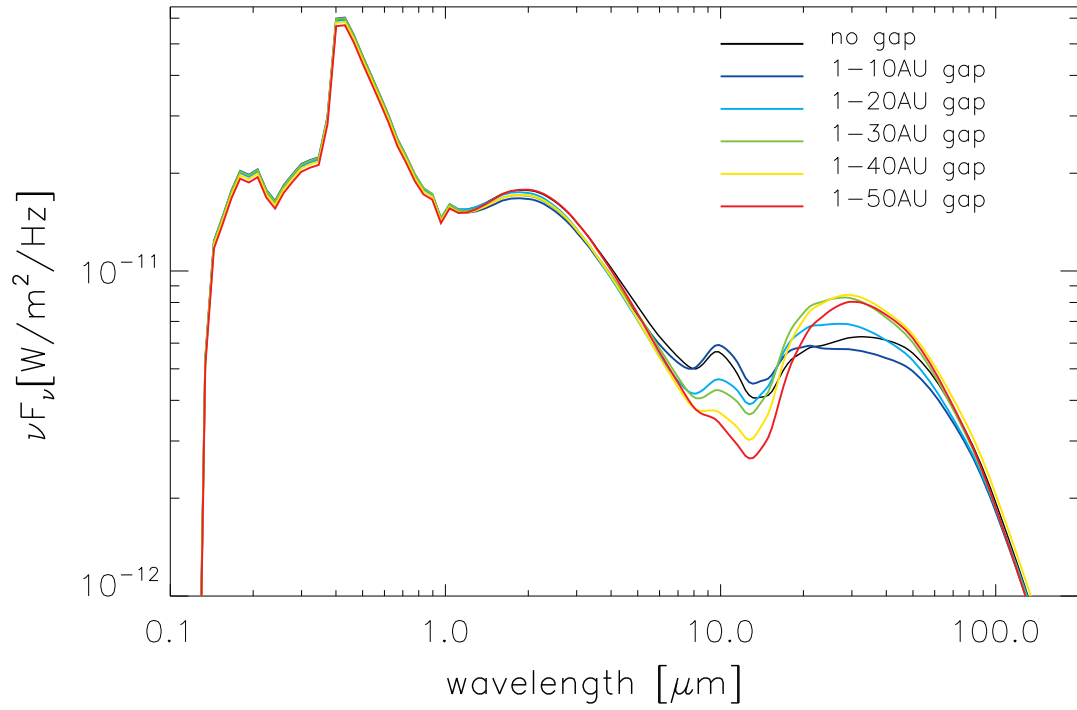


FIG. 5.— SEDs of each models shown in Fig. 4.

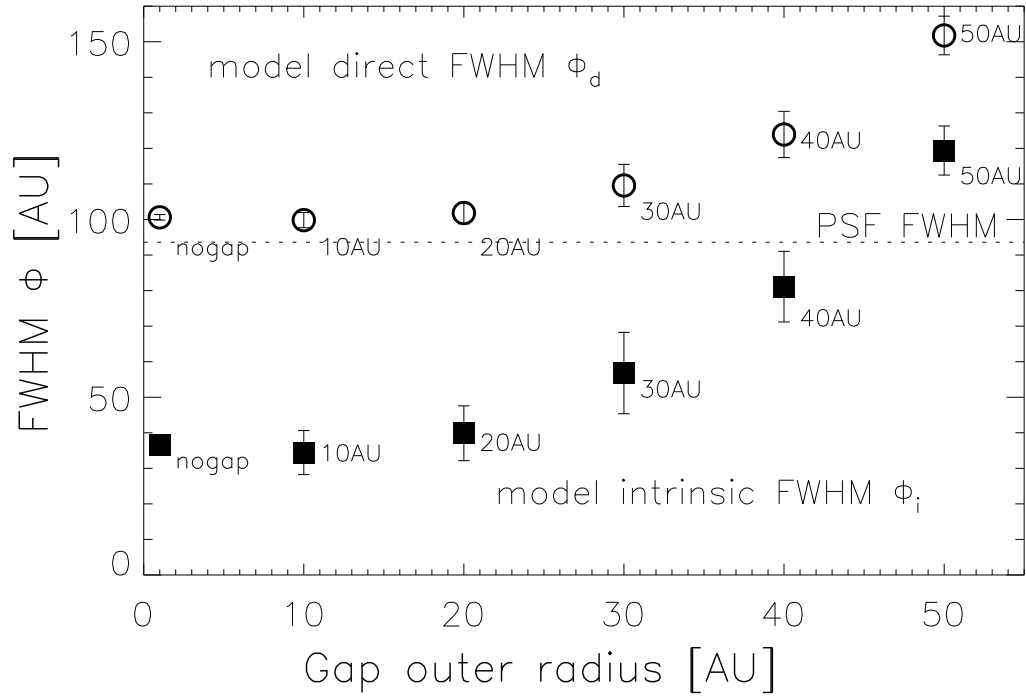


FIG. 6.— The direct FWHM Φ_d of the PSF convolved model image shown in Fig. 4 plotted against the outer gap radius. Similar plot of intrinsic FWHM Φ_i derived via quadratic subtraction method is also shown. Disks with large gap (gap outer radius is larger than 20 AU) show larger FWHM values than those with no or small gap.

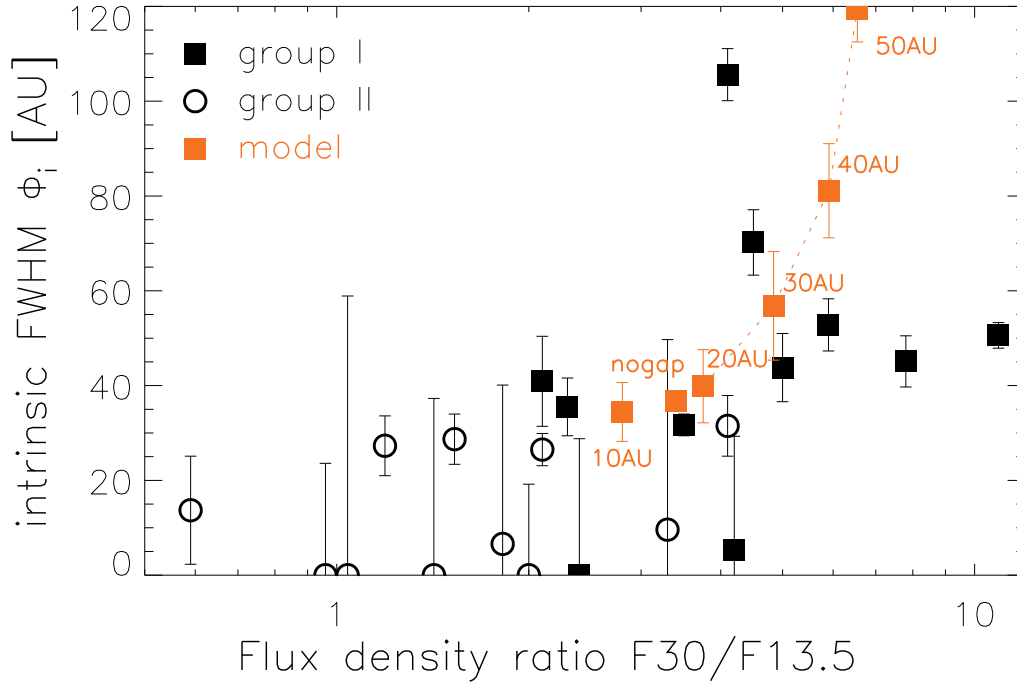


FIG. 7.— Plot of intrinsic FWHM Φ_i of the model (red) against the MIR color overplotted in Fig.3. Again, disks with large gap (gap outer radius is larger than 20 AU) show larger MIR index $[30/13.5]$ than those with no or small gap. In other words, redder sources show more extended emission.